SCIENTIFIC REPORTS

OPEN

CONFERENCE PROCEEDINGS

ACSMS2014

SUBJECT AREAS:
NANOPARTICLES
METAL-ORGANIC FRAMEWORKS

Received
13 August 2014

Accepted
22 October 2014

Published
10 November 2014

Correspondence and requests for materials should be addressed to K.C.-W.W. (kevinwu@ntu.edu.tw)

# Platinum-Free Counter Electrode Comprised of Metal-Organic-Framework (MOF)-Derived Cobalt Sulfide Nanoparticles for Efficient Dye-Sensitized Solar Cells (DSSCs)

Shao-Hui Hsu[1], Chun-Ting Li[1], Heng-Ta Chien[1], Rahul R. Salunkhe[2], Norihiro Suzuki[3], Yusuke Yamauchi[2], Kuo-Chuan Ho[1] & Kevin C.-W. Wu[1]

[1]Department of Chemical Engineering, National Taiwan University, No. 1, Sec. 4 Roosevelt Road, Taipei 10617, Taiwan, [2]World Premier International (WPI) Research Center for Materials Nanoarchitectonics (MANA), National Institute for Materials Science (NIMS), 1-1 Namiki, Tsukuba, Ibaraki 305-0044, Japan, [3]International Center for Young Scientists (ICYS), National Institute for Materials Science (NIMS), 1-2-1 Sengen, Tsukuba, Ibaraki 305-0047, Japan.

**We fabricated a highly efficient (with a solar-to-electricity conversion efficiency (η) of 8.1%) Pt-free dye-sensitized solar cell (DSSC). The counter electrode was made of cobalt sulfide (CoS) nanoparticles synthesized via surfactant-assisted preparation of a metal organic framework, ZIF-67, with controllable particle sizes (50 to 320 nm) and subsequent oxidation and sulfide conversion. In contrast to conventional Pt counter electrodes, the synthesized CoS nanoparticles exhibited higher external surface areas and roughness factors, as evidenced by X-ray diffraction (XRD), scanning electron microscopy (SEM) element mapping, and electrochemical analysis. Incident photon-to-current conversion efficiency (IPCE) results showed an increase in the open circuit voltage ($V_{OC}$) and a decrease in the short-circuit photocurrent density (Jsc) for CoS-based DSSCs compared to Pt-based DSSCs, resulting in a similar power conversion efficiency. The CoS-based DSSC fabricated in the study show great potential for economically friendly production of Pt-free DSSCs.**

Solar energy is considered one of the most potential energy sources to replace petroleum[1]. So far, scientists have been working on the development of various kinds of cells that can convert solar energy into electricity, and the cells that have been developed include silicon solar cells[2], organic solar cells[3,4], quantum dot solar cells[5–7], dye-sensitized solar cells (DSSCs)[1,8,9], and so on. Among these photovoltaic cells, DSSCs have attracted much attention because of their low manufacturing cost, simple fabrication process, and durability for conventional roll-printing technologies that are not applicable to glass-based systems[1]. In general, a regular DSSC device consists of dye molecules, electrolyte, a spacer, working electrode, and counter electrode (CE). Recent studies of DSSCs have focused on several issues including (1) the synthesis of new dye molecules that can absorb all solar light wavelengths[10], (2) the fabrication of new hierarchically titania materials for the working electrode[11], (3) the development of solid state DSSCs using a hybrid perovskite $CH_3NH_3PbI_3$ dye[12], and (4) the replacement of platinum (Pt) counter electrodes[13].

Although platinum owns outstanding catalytic property in DSSCs[14,15], platinum is a noble metal and very rare on earth that leads high price in the market. In order to reduce production costs and to popularize DSSCs, it is necessary to use cheaper materials with similar performances to replace Pt. So far, several kinds of alternatives such as conducting polymers[16,17], carbon[18–20], and transition metal-containing materials[21,22] have been proposed in the literature to replace Pt counter electrodes. An ideal substitute for Pt must exhibit superior conductivity, stability, and electrocatalytic ability for reduction of the electrolyte (i.e. $I_3^-$). Considering these requirements, cobalt sulfide (CoS) has been regarded as one of the most promising candidates[13,23,24]. The Grätzel group reported the first synthesis of a CoS counter electrode by an electrochemical deposition method[13]. The efficiency of CoS-based DSSCs was 6.5%, which is comparable to that of Pt-based DSSCs. Our group also reported the synthesis of

one-dimensional CoS acicular nanorod arrays through a sequential chemical bath deposition (CBD) and conversion process, and the corresponding CoS-based DSSCs showed an efficiency of 7.67%. This value was nearly the same efficiency of Pt-based DSSCs (7.70%)[23]. With measurements of cyclic voltammetry and Tafel polarization curve, we further concluded that the electrocatalytic ability of the synthesized CoS acicular nanorod arrays was superior to that of conventional Pt for the reduction of $I_3^-$. Although this method generate one-dimensional CoS acicular nanorod arrays, the thickness of the CoS arrays is difficult to control. Considering the feasibility of fabrication processes, the morphology of powder is superior to those of arrays or thin films. Moreover, in order to increase the surface area of CoS powder, the synthesis of CoS nanoparticles with controllable particle size is in great demand.

Metal-organic frameworks (MOFs), which consist of metal cations and organic ligands, possess unique structural topologies and tunable functionalities that are useful for gas absorption[25–27], separation[28,29], catalyst[30,31], sensors[32], dye degradation[33], bio-imaging[34], and so on. A new sub-family of MOF, namely zeolitic-imidazole frameworks (ZIFs), is topologically isomorphic with zeolites. Depending on the metal cations used in the synthesis, the corresponding ZIFs will exhibit the intrinsic properties of the metal cation. Furthermore, after thermal treatments in a nitrogen or oxygen atmosphere, ZIFs will convert to the corresponding metal or metal oxides, respectively[35,36]. For example, ZIF-67 consists of cobalt cations (as the metal source) and 2-methylimidazole (mIm, as the organic ligand), which assemble into a rhombic dodecahedral morphology (so called sodalite (SOD) topology) with a pore size of around 0.34 nm. After calcination in an oxygen atmosphere, the cobalt-mIm framework will convert to CoOx[36].

Here, in order to prepare a new material to replace Pt for DSSC applications, our approach is to further convert CoOx to CoS through a simple sulfide conversion, as shown in Fig. 1. In addition, we aim to synthesize CoS nanoparticles that are as small as possible, because smaller nanoparticles will exhibit more external surface area and excellent dispersion, thus promoting catalytic ability. Particle sizes of ZIF-67 are successfully controlled in the range of 50–320 nm by the addition of a surfactant named CTAB. The effect of particle size on the film thickness of the ZIF-67-derived CoS was studied. We then evaluate the fabricated CoS nanoparticles as a cathode for DSSCs. Finally a series of DSSC analyses exhibits high open circuit voltage ($V_{oc}$, 0.78 V) and fill factor (FF, 71%) in DSSCs. Most importantly, the highest power (photon-to-electron) conversion efficiency (8.1%) from CoS-derived DSSCs is the same as that from Pt-based DSSCs (8.0%). We believe that the high performance of CoS-derived DSSCs here is attributed to the successful synthesis of smaller CoS nanoparticles.

## Results

As seen in the field-emission scanning electron microscopy (FE-SEM) image (Fig. 2a) and transmission electron microscopy (TEM) image (Supporting Information), the size of regular ZIF-67 nanoparticles is 320 nm when no CTAB was added. After the addition of CTAB (0.01 wt%), the particle size decreased to around 200 nm, as shown in Fig. 2b. When the amount of CTAB increased to 0.0625 wt%, the particle size further decreased to around 50 nm, and the morphology became an irregular shape, as shown in Fig. 2c. The relationship between the addition of CTAB and the particle size of ZIF-67 was summarized in Fig. 2d.

After oxidation of ZIF-67 and sulfide conversion of cobalt oxide, the surface morphology and the corresponding element distribution of the synthesized cobalt oxide (Fig. 3a) and cobalt sulfide (Fig. 3b) were examined with FE-SEM and energy-dispersive X-ray spectroscopy (EDS), respectively. The XRD patterns of $Co_3O_4$ and CoS films shown in Fig. 4 clearly evidence different crystalline phases for $Co_3O_4$ ($Co_3O_4$-0.0625) and CoS (CoS-0.0625).

Figure 5 shows the current density to voltage (*J-V*) characteristics of DSSC with various CE materials. The open circuit potential ($V_{oc}$), short circuit current density ($J_{sc}$), fill factor (FF), and energy conversion efficiency ($\eta$) of DSSC cell with various CE materials are then summarized in the inset of Fig. 5. The CoS nanoparticles converted from ZIF-67 with different particle sizes were then used as CE materials, and their *J-V* characteristics of the corresponding DSSCs are shown in Fig 6. The systematic detail parameters are summarized in the inset of Fig. 6.

## Discussion

To control the particle size of the synthesized ZIF-67, we have adopted the concept of using a surfactant (here we use CTAB) as a dispersant because it has been applied to control the particle size of ZIF-8[37]. Adding surfactant is a common strategy to control particle size and morphology. The most important consideration of surfactant addition is the interaction between metal ion and surfactant slow reaction of metal and organic molecule, resulting slow nucleation and controllable crystal growth[37,38]. We added various amounts of CTAB into the synthetic systems, and the resulting samples were observed with SEM. As shown SEM image in Fig. 2a and TEM image in Supporting Information Fig. S1, regular ZIF-67 nanoparticles with a rhombic dodecahedron shape and an average particle size of 320 nm were obtained when no CTAB was added. After the addition

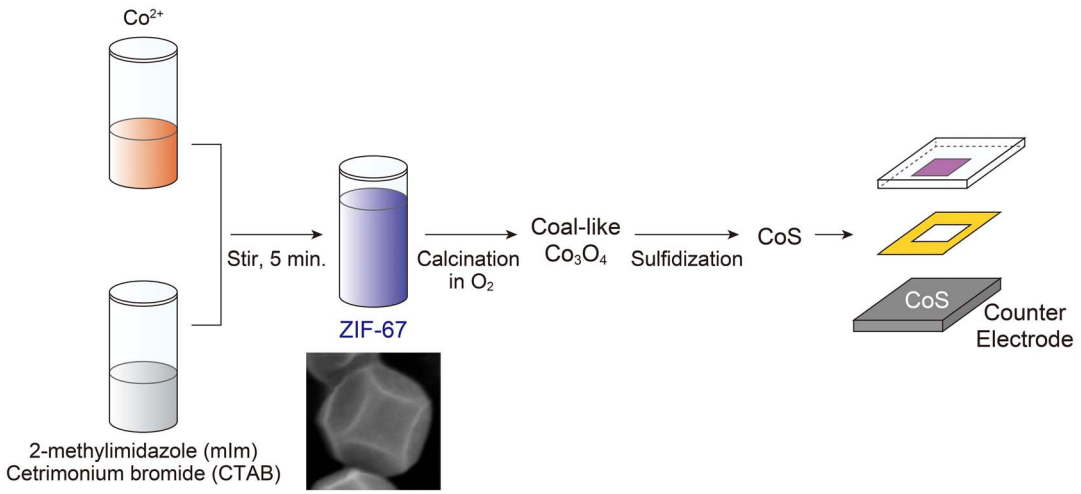


**Figure 1 | Schematic of the fabrication procedure of cobalt sulfide as Pt-replaced counter electrode for dye-sensitized solar cells.**

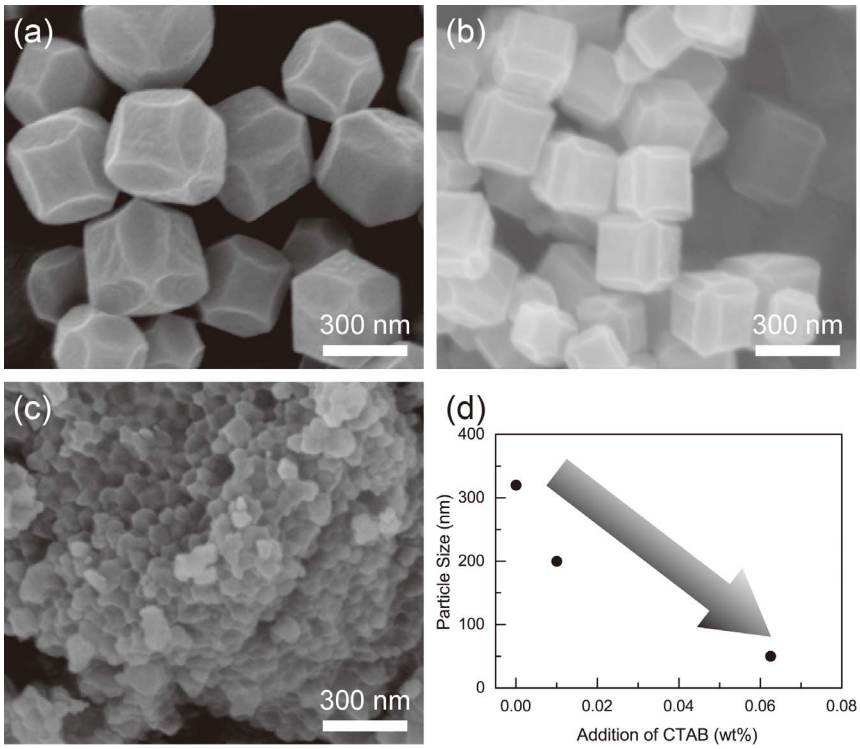


**Figure 2** | **SEM images of (a) ZIF-67 without addition of CATB, (b) ZIF-67 with 0.01 wt% CTAB addition, (c) ZIF-67 with 0.0625 wt% CTAB addition, and (d) the relationship between the amount of CTAB added and the corresponding particle size.**

of CTAB (0.01 wt%), the particle size decreased to around 200 nm and the morphology changed to cubic with {110} facets, as shown in Fig. 2b. According to a previous report by the Lai's group, the interaction energies of the {100}, {110}, and {111} facets of ZIF-8 are -774.56, -394.91, and -104.21 kcal $mol^{-1}$, respectively[37], indicating that the CTAB molecules absorb more easily to the {100} than to other facets to block the sites for growth of $Co^{2+}$ and 2-methylimidazole, resulting in a cubic morphology.

When the amount of CTAB was increased to 0.0625 wt%, the particle size decreased further to around 50 nm, and the morphology became irregular, as shown in Fig. 2c. These results indicate that addition of CTAB is an efficient way to precisely control the particle size of ZIF-67. The crystallinities of the three samples were analyzed by XRD (Supporting Information Fig. S2), and all samples exhibited the same XRD peak positions as those of simulated ZIF-67 (CCDC #671073). This result indicates that the synthesized ZIF-67 samples have highly crystalline structures. In addition, compared to the XRD patterns of ZIF-67 (no CTAB addition), the XRD patterns of ZIF-67 (with 0.01 wt% and 0.0625 wt% CTAB) revealed a greatly decrease in the (110) ($2\theta = 7.4$ degree) peak as well as (200) ($2\theta = 10.3$ degree) and a significant increase in the (222) ($2\theta = 18.0$ degree) peak of ZIF-67-0.0625. These evidences agree with the interaction energies between CTAB and crystal faces through molecular dynamics (MD) simulations that face with lower interaction energy. Based

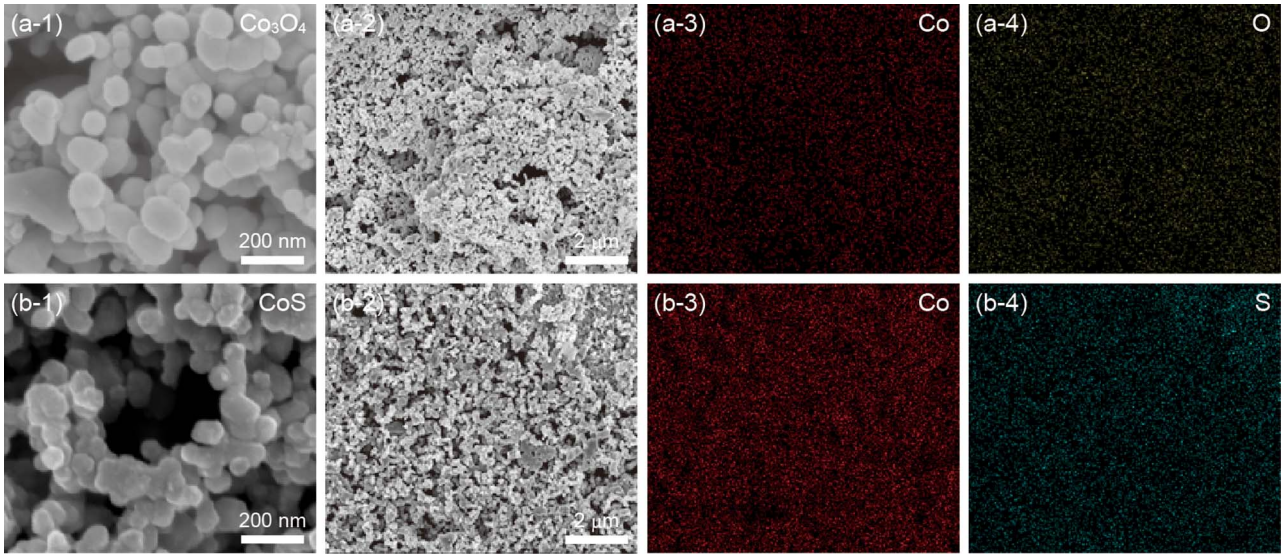


**Figure 3** | **SEM images of (a) $Co_3O_4$-0.0625 on FTO and (b) CoS-0.0625 on FTO; (a-1) and (b-1) are SEM images at 150,000×, (a-2) and (b-2) are SEM images at 30,000× magnification, (a-3), (a-4), (b3), and (b-4) are element mapping results of Co, O, and S.**

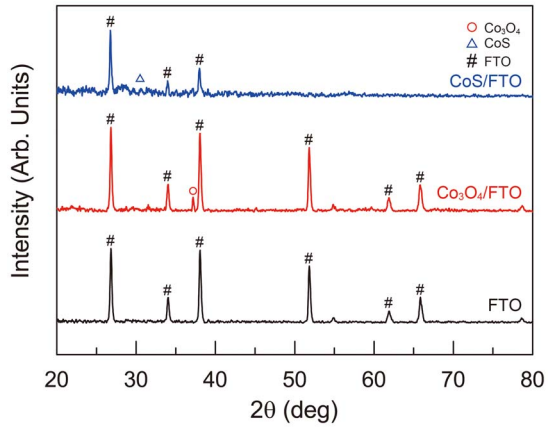


**Figure 4 | XRD patterns of the bare FTO substrate, $Co_3O_4$ on FTO, and CoS on FTO.**

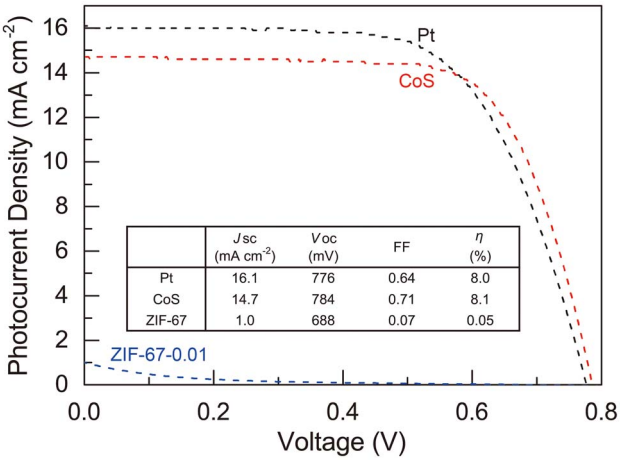


| | Jsc (mA cm$^{-2}$) | Voc (mV) | FF | η (%) |
|---|---|---|---|---|
| Pt | 16.1 | 776 | 0.64 | 8.0 |
| CoS | 14.7 | 784 | 0.71 | 8.1 |
| ZIF-67 | 1.0 | 688 | 0.07 | 0.05 |

**Figure 5 | *J-V* curves of the DSSCs with ZIF-67, CoS and sputtered Pt measured under a light intensity of 100 mW/cm².** The table in the inset lists the detailed information of Pt, CoS, ZIF-67-based DSSCs.

on Wulff's construction, the equilibrium shape of crystal depends on energy minimization of certain crystal planes. The anisotropic growth of ZIF-67 is present in the case of CTAB addition, which indicates that CTAB serves as a capping agent to control the growth of ZIF-67 that leads rhombic dodecahedral and cubic morphology. In the case of 0.01 wt% CTAB addition, the moderate amount of CTAB can selectively absorb to the facets with lowest interaction force, {100}, resulting in decreased intensity of the XRD peak (100). When more CTAB (0.0625 wt%) is added to the precursor solution, the corresponding XRD peaks decreased except for the (211) peak. We suggest this was because CTAB can be absorbed to the many facets of ZIF-67, thus inhibiting the growth of ZIF-67 and separating the ZIF-67 nanoparticles to further control the crystal morphology and size.

After deposition of $Co_3O_4$ or CoS nanoparticles on FTO substrates, both samples showed porous film structures from top view SEM images (Fig. 3a-1, 2 and Fig. 3b-1, 2), implying that the electrolyte can penetrate through the film easily. In order to demonstrate that the $Co_3O_4$ or CoS nanoparticles were homogeneously distributed on the substrate, EDS mapping in Fig. 3a-3, 4 and Fig. 3b-3, 4 revealed that Co and O elements (for $Co_3O_4$) and Co and S elements (for CoS), respectively, were uniformly located on the all powders. The estimated Co and O amounts for $Co_3O_4$ were 39 atom% and 49 atom%, and Co and S amounts for CoS were 39 atom% and 21 atom%. Furthermore, the XRD patterns of $Co_3O_4$ and CoS films in Fig. 4 clearly show different crystalline phases for $Co_3O_4$ ($Co_3O_4$-0.0625) and CoS (CoS-0.0625), indicating a successful $Co_3O_4$-to-CoS conversion. According to Joint Committee on Powder Diffraction Standards (JCPDS, PDF no. 80-1545, $Co_3O_4$, and JCPDS 75-0605, CoS), $Co_3O_4$/FTO has a cobalt oxide phase, while CoS/FTO barely has any cobalt oxide phase due to full conversion to the CoS phase. Based on the characterizations above, we believe that the CoS film was successfully attained.

Various materials used for counter electrodes (CE) in DSSC devices have been studied, while keeping the working electrode and electrolyte the same. Platinum has good catalytic properties and is usually used for the counter electrode to reduce $I_3^-$. As shown in the table in Fig. 5, the power efficiency of the DSSC with CoS-based CE was higher than that of the cells with Pt-based CE, due to the higher value of $V_{oc}$ and improved FF. In contrast, the cell efficiency using ZIF-67-based CE was much lower than those of Pt and CoS-based DSSCs. The low efficiency of ZIF-67-based DSSCs results from the low current density that is due to the poor electron conductivity of ZIF-67. Compared to Pt-based DSSCs, CoS-based DSSCs have improved open circuit potential ($V_{oc}$) by using CoS as a counter electrode. It is known that open-circuit voltage is the difference between the Fermi level of the nanocrystalline $TiO_2$ film and the redox potential of the mediator that is influenced by instinct material properties of the counter electrodes. The superior FF of CoS-based DSSCs leads to an enhanced power conversion efficiency. In fact, the reason for the high FF value is closely related to low series resistance ($R_s$), which is composed of the TCO substrate resistance ($R_{TCO}$), diffusion resistance of $I_3^-$ ions in electrolyte ($R_E$), and charge-transfer resistance ($R_{CT}$) at the interface of the counter electrode and electrolyte in the DSSC[39]. In this case, the $R_{TCO}$ and $R_E$ of CoS-based DSSCs are the same as those of Pt-based DSSCs[40,41]. Therefore, the lower $R_{CT}$ of CoS led to higher $R_s$, resulting in increased FF of the CoS-based DSSC.

The roughness factor (RF) of the counter electrode affects the $R_{CT}$ value. RF is defined as the ratio of an effective actual surface to the projected area of the counter electrode that can present the effective activity area for $I_3^-$ reduction. Therefore, $R_{CT}$ decreases with increasing RF. In this study, the RF value in the Pt-based DSSC is equal to one because Pt/FTO is made by sputtering, leading to a planar Pt structure on the FTO glass. On the other hand, the RF value in the CoS-based DSSC is larger than one because CoS nanoparticles were coated on the FTO glass. In our previous report, we prepared an one-dimensional cobalt sulfide acicular nanorod arrays (CoS-ANARS/FTO) on a fluorine-doped tin oxide substrate[23]. The best FF value of

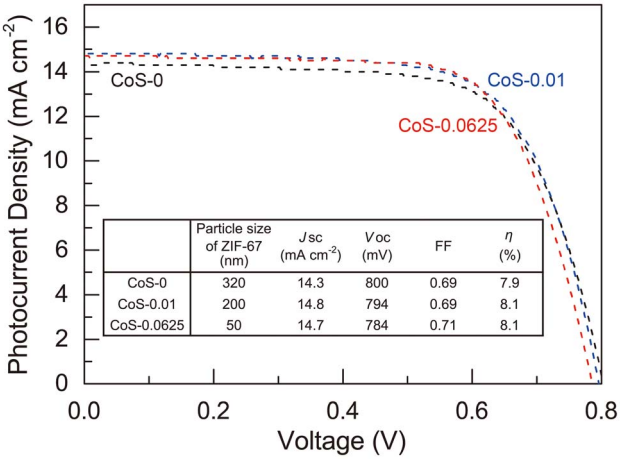


| | Particle size of ZIF-67 (nm) | Jsc (mA cm$^{-2}$) | Voc (mV) | FF | η (%) |
|---|---|---|---|---|---|
| CoS-0 | 320 | 14.3 | 800 | 0.69 | 7.9 |
| CoS-0.01 | 200 | 14.8 | 794 | 0.69 | 8.1 |
| CoS-0.0625 | 50 | 14.7 | 784 | 0.71 | 8.1 |

**Figure 6 | *J-V* curves of the CoS-based DSSCs with 320 nm, 200 nm, and 50 nm ZIF-67 nanoparticles as precursors measured under a light intensity of 100 mW/cm².** The table in the inset lists the detailed information of DSSCs with CoS-x (x indicates different particle size of ZIF-67) as counter electrodes.

the CoS-ANARS/FTO-based DSSC was 0.66, lower than that of CoS/FTO (FF = 0.71), due to the lower RF value.

The effect of CoS particle size on the performance of the corresponding CoS-based DSSCs was studied. As discussed previously, we have successfully controlled the particle size of ZIF-67 in the range of 50 to 320 nm by using CTAB as the capping reagent. The systematic detail parameters, and the *J-V* characteristics of the corresponding DSSCs with different particle sizes are summarized in the inset of Fig. 6. As shown in the table, the power conversion efficiency increases as the particle size of CoS deceases. We suggest that smaller CoS nanoparticles exhibit more active sites for reacting with $I_3^-$. Therefore, the DSSC with the smallest CoS nanoparticle (i.e. CoS-0.0625) exhibited the highest efficiency with a value of 8.1%. The complete device characteristics are as follows: $V_{OC}$ = 0.784 V, $J_{SC}$ = 14.7 mA $cm^{-2}$, and FF = 0.71. The performance of our CoS-based DSSC is close to that of Pt-based DSSC, indicating that our synthesized CoS materials have great potential to replace Pt for future Pt-free DSSC devices.

In summary, CoS nanoparticles of different sizes were successfully synthesized through the CTAB-assisted preparation of a metal organic framework, ZIF-67, and subsequent oxidation and sulfide conversion to CoS. The generated CoS nanoparticles were then coated onto FTO substrates and used as an efficient counter electrode for DSSCs. The small nanoparticle size enhanced interaction with dye molecules and increased roughness factor. The enhanced $V_{OC}$ value of the CoS-based DSSCs resulted in greater fill factor value, leading to an improved efficiency of 8.1%. This value is comparable to that of Pt-based DSSCs (i.e. 8.0%), indicating that the synthesized CoS nanoparticles can replace Pt and serve as an efficient couter electrode material for next-generation economically available DSSCs.

## Methods

**Preparation of N719-sensitized $TiO_2$ working electrode.** A $TiO_2$ colloid was synthesized by adding TTIP (0.5 M, 72 mL) to a nitric acid (0.1 M, 430 mL) aqueous solution with constant stirring and heating at 88°C for 8 h. In order to further promote the uniform growth of $TiO_2$ nanoparticles (up to ca. 20 nm), the system was transferred to an autoclave (PARR 4540, U.S.A.). After heating at 240°C for 12 h, the $TiO_2$ colloid solution was concentrated to $TiO_2$ nanoparticles at a concentration of 8 wt% (with respect to the original $TiO_2$ colloid). The scattering layer paste (SL paste) was prepared by adding PEG (25 wt%) and ST–41 (100 wt%) (with respect to the weight of the $TiO_2$ nanoparticles) into the concentrated-$TiO_2$ nanoparticles to prevent aggregation of the $TiO_2$ nanoparticles and to reduce light loss, respectively. In the next stage, the $TiO_2$ photoanode was prepared by using the transparent layer and scattering layer pastes as prepared previously. Fluorine–doped $SnO_2$ (FTO, TEC–7, 7 Ω sq.–1, NSG America, Inc., New Jersey, USA) conducting glass was first cleaned with a neutral cleaner and then washed sequentially with de-ionized water, acetone, and isopropanol. The conducting surface of the FTO was treated with a solution of TTIP and 2-methoxyethanol (weight ratio of 1 : 3) to obtain a good mechanical contact layer between the conducting glass and the $TiO_2$ film. A porous $TiO_2$ film of thickness around 15 μm was coated on the pre-cleaned FTO by the doctor blade technique, and consisted of two $TiO_2$ layers: a transparent layer (thickness of about 10 μm) and a scattering layer (thickness of about 5 μm). Each $TiO_2$ layer was sintered at 500°C for 30 min in an air atmosphere. After the sintering process, we used the prepared $TiO_2$ photoanode with a constant active area of 0.16 $cm^2$ and immersed the photoanode in a N719 dye solution ($5 \times 10^{-4}$ M) at room temperature for 24 hrs. N719 dye was dissolved in ACN and tBA (volume ratio of 1 : 1) as a standard dye solution. Besides, the transparent layer paste (TL paste, Ti-nanoxide HT/SP, 13 nm) was purchased from Solaronix, S.A., Aubonne, Switzerland.

**Synthesis of CoS nanoparticles and its counter electrode.** ZIF-67 with controllable particle size was synthesized via an aqueous solution method. Typically, $CoCl_2 \cdot 6H_2O$ (5 mM) was dissolved in de-ionized water. An aqueous solution of 2-methylimidazole (3.45 M) with or without cetyl trimethylammonium bromide (CTAB) (0.01 or 0.0625 wt%) was also prepared. The above-mentioned two solutions were then mixed vigorously for 5 minutes, and the resulting purple precipitates were collected by centrifugation, washed with water several times, and finally dried in vacuum for one day. The obtained products were denoted as ZIF-67-0, ZIF-67-0.01, and ZIF-67-0.0625 for the amounts of CTAB (0, 0.01, and 0.0625 wt%, respectively). In order to convert ZIF-67 into cobalt oxide, the synthesized ZIF-67 powders were then directly calcined under oxygen flow at 600°C for three hours. The temperatures inside the furnace were gradually increased from room temperature to a target temperature at a heating rate of 5°C $min^{-1}$. After the calcination process, the paste containing the resulting cobalt oxide ($Co_3O_4$), ethyl cellulose, and alpha-terpineol was prepared for film deposition on FTO via the doctor blade method. The obtained $Co_3O_4$/FTO thin film was then calcined at 450°C for 30 min at a heating rate of 5°C $min^{-1}$. The sulfide conversion process was performed by putting the $Co_3O_4$/FTO film in a sodium sulfide aqueous solution (0.01 M) at 90°C for 24 hours. After the sulfide conversion process, the obtained cobalt sulfide (CoS) film was washed with DI water and dried at 60°C before it was used as a counter electrode for DSSCs.

**Preparation of Pt counter electrode.** The standard Pt CE was prepared by DC-sputtering. A Pt thin film of thickness 50 nm on a fluorine-doped $SnO_2$ substrate was prepared.

**Assembly of dye-sensitized solar cells.** The DSSC device was composed of the $TiO_2$ photoanode coupled with the CE. The distance between these two electrodes was fixed and sealed by heating a thick Surlyn® (60 μm). The electrolyte, which contained LiI (0.1 M), DMPII (0.6 M), $I_2$ (0.05 M), and tBP (0.5 M) in MPN/ACN (1 : 1 in volume ratio), was injected into the gap between these two electrodes by capillarity.

**Photovoltaic measurements.** The power conversion efficiency of DSSCs was obtained under 100 mW $cm^{-2}$ light illumination by a class-A quality solar simulator (XES–301S, AM1.5G, San–Ei Electric Co., Ltd., Osaka, Japan). The intensity of the incident light was calibrated with a standard Si cell (PECSI01, Peccell Technologies, Inc., Kanagawa, Japan).


1. Grätzel, M. Photoelectrochemical cells. *Nature* **414**, 338–344 (2001).
2. Tsakalakos, L., Balch, J., Fronheiser, J., Korevaar, B. A., Sulima, O. & Rand, J. Silicon nanowire solar cells. *Appl. Phys. Lett.* **91**, 233117 (2007).
3. Weickert, J. & Schmidt-Mende, L. Perspective: Hybride solar cells: How to get the polymer to cooperate? *APL Mat.* **1**, 020901–020903 (2013).
4. Hoppe, H. & Sariciftci, N. S. Organic solar cells: An overview. *J. Mater. Res.* **19**, 1924–1945 (2004).
5. Kongkanand, A., Tvrdy, K., Takechi, K., Kuno, M. & Kamat, P. V. Quantum dot solar cells. Tuning photoresponse through size and shape control of CdSe-$TiO_2$ architecture. *J. Am. Chem. Soc.* **130**, 4007–4015 (2008).
6. Rao, H.-S. *et al.* CdS/CdSe co-sensitized vertically aligned anatase $TiO_2$ nanowire arrays for efficient solar cells. *Nano Energy* **8**, 1–8 (2014).
7. Hsu, S.-H., Hung, S.-F. & Chien, S.-H. CdS sensitized vertically aligned single crystal $TiO_2$ nanorods on transparent conducting glass with improved solar cell efficiency and stability using ZnS passivation layer. *J. Power Sources* **233**, 236–243 (2013).
8. Bijarbooneh, F. H. *et al.* Structurally stabilized mesoporous TiO2 nanofibres for efficient dye-sensitized solar cells *APL Mat.* **1**, 032106–032112 (2013).
9. Chung, I., Lee, B., He, J., Chang, R. P. H. & Kanatzidis, M. G. All-solid-state dye-sensitized solar cells with high efficiency. *Nature* **485**, 486–489 (2012).
10. Li, C., Wang, W., Wang, X., Zhang, B. & Cao, Y. Molecular Design of Squaraine Dyes for Efficient Far-red and Near-IR Sensitization of Solar Cells. *Chem. Lett.* **34**, 554–555 (2005).
11. Ito, S. *et al.* Fabrication of thin film dye sensitized solar cells with solar to electric power conversion efficiency over 10%. *Thin Solid Films* **516**, 4613–4619 (2008).
12. Liu, M., Johnston, M. B. & Snaith, H. J. Efficient planar heterojunction perovskite solar cells by vapour deposition. *Nature* **501**, 395–398 (2013).
13. Wang, M. *et al.* CoS Supersedes Pt as Efficient Electrocatalyst for Triiodide Reduction in Dye-Sensitized Solar Cells. *J. Am. Chem. Soc.* **131**, 15976–15977 (2009).
14. Lin, J. *et al.* Highly connected hierarchical textured $TiO_2$ spheres as photoanodes for dye-sensitized solar cells. *J. Mater. Chem. A* **2**, 8902–8909 (2014).
15. Lin, J. *et al.* 3D hierarchical rutile $TiO_2$ and metal-free organic sensitizer producing dye-sensitized solar cells 8.6% conversion efficiency. *Sci. Rep.* **4**, 5769–8916 (2014).
16. Tai, Q. *et al.* In situ prepared transparent polyaniline electrode and its application in bifacial dye-sensitized solar cells. *ACS Nano* **5**, 3795–3799 (2011).
17. Wu, J. *et al.* High-performance polypyrrole nanoparticles counter electrode for dye-sensitized solar cells. *J. Power Sources* **181**, 172–176 (2008).
18. Li, G.-R., Wang, F., Jiang, Q.-W., Gao, X.-P. & Shen, P.-W. Carbon nanotubes with titanium nitride as a low cost counter electrode material for dye sensitized solar cells. *Angew. Chem. Int. Ed.* **49**, 3653–3656 (2010).
19. Cha, S. I., Koo, B. K., Seo, S. H. & Lee, D. Y. Pt-free transparent counter electrodes for dye-sensitized solar cells prepared from carbon nanotube micro-balls. *J. Mater. Chem.* **20**, 659–662 (2010).
20. Wu, M., Lin, X., Hagfeldt, A. & Ma, T. Low-cost molybdenum carbide and tungsten carbide counter electrodes for dye-sensitized solar cells. *Angew. Chem. Int. Ed.* **50**, 3520–3524 (2011).
21. Gong, F., Wang, H., Xu, X., Zhou, G. & Wang, Z.-S. In situ growth of $Co_{0.85}Se$ and $Ni_{0.85}Se$ on conductive substrates as high-performance counter electrodes for dye-sensitized solar cells. *J. Am. Chem. Soc.* **134**, 10953–10958 (2012).
22. Wu, M. *et al.* Economical Pt-free catalysts for counter electrodes of dye-sensitized solar cells. *J. Am. Chem. Soc.* **134**, 3419–3428 (2012).
23. Kung, C.-W. *et al.* CoS acicular nanorod arrays for the counter electrode of an efficient dye-sensitized solar cell. *ACS Nano* **6**, 7016–7025 (2012).
24. Lin, J.-Y. & Liao, J.-H. Mesoporous electrodeposited-CoS film as a counter electrode catalyst in dye-sensitized solar cells. *J. Electrochem. Soc.* **159**, D65–D71 (2012).

25. Lee, H. J., Cho, W., Lim, E. & Oh, M. One-pot synthesis of magnetic particle-embedded porous carbon composites from metal–organic frameworks and their sorption properties. *Chem. Commun.* **50**, 5476–5479 (2014).
26. Srinivas, G., Krungleviciute, V., Guo, Z.-X. & Yildirim, T. Exceptional $CO_2$ capture in a hierarchically porous carbon with simultaneous high surface area and pore volume. *Energy Environ. Sci.* **7**, 335–342 (2014).
27. Hinterholzinger, F. M. *et al*. One-dimensional metal–organic framework photonic crystals used as platforms for vapor sorption. *J. Mater. Chem.* **22**, 10356–10362 (2012).
28. Chaikittisilp, W., Ariga, K. & Yamauchi, Y. A new family of carbon materials: synthesis of MOF-derived nanoporous carbons and their promising applications. *J. Mater. Chem. A* **1**, 14–19 (2013).
29. Ordoñez, M. J. C., Balkus, K. J., Jr., Ferraris, J. P. & Musselman, I. H. Molecular sieving realized with ZIF-8/Matrimid® mixed-matrix membranes. *J. Membr.Sci.* **361**, 28–37 (2010).
30. Fu, Y. *et al.* An amine-functionalized titanium metal-organic framework photocatalyst with visible-light-induced activity for $CO_2$ reduction. *Angew. Chem. Int. Ed.* **51**, 3364–3367 (2012).
31. Sabo, M., Henschel, A., Fröde, H., Klemm, E. & Kaskel, S. Solution infiltration of palladium into MOF-5: synthesis, physisorption and catalytic properties. *J. Mater. Chem.* **17**, 3827–3832 (2007).
32. Liu, S., Xiang, Z., Hu, Z., Zheng, X. & Cao, D. Zeolitic imidazolate framework-8 as a luminescent material for the sensing of metal ions and small molecules. *J. Mater. Chem.* **21**, 6649–6653 (2011).
33. Torad, N. L. *et al.* Direct synthesis of MOF-derived nanoporous carbon with magnetic Co nanoparticles toward efficient water treatment. *Small* **10**, 2096–2107 (2014).
34. Rocca, J. D., Liu, D. & Lin, W. Nanoscale Metal–organic frameworks for biomedical imaging and drug delivery. *Acc. Chem. Res.* **44**, 957–968 (2011).
35. Yang, S. J. *et al*. MOF-derived hierarchically porous carbon with exceptional porosity and hydrogen storage capacity. *Chem. Mater.* **24**, 464–470 (2012).
36. Wu, R. *et al*. Zeolitic imidazolate framework 67-derived high symmetric porous $Co_3O_4$ hollow dodecahedra with highly enhanced lithium storage capability. *Small* **10**, 1932–1938 (2014).
37. Pan, Y. *et al.* Tuning the crystal morphology and size of zeolitic imidazolate framework-8 in aqueous solution by surfactants. *CrystEngComm* **13**, 6937–6940 (2011).
38. Hu, M., Ishihara, S., Ariga, K., Imura, M. & Yamauchi, Y. Kinetically controlled crystallization for synthesis of monodispersed coordination polymer nanocubes and their self assembly to periodic arrangements. *Chem. Eur. J.* **19**, 1882–1885 (2013).
39. Han, L., Koide, N., Chiba, Y. & Mitate, T. Modeling of an equivalent circuit for dye-sensitized solar cells. *Appl. Phys. Lett.* **84**, 2433–2435 (2004).
40. Kron, G., Rau, U. & Werner, J. H. Influence of the built-in voltage on the fill factor of dye-sensitized solar cells. *J. Phys. Chem. B* **107**, 13258–13261 (2003).
41. Lee, W. J., Ramasamy, E., Lee, D. Y. & Song, J. S. Dye-sensitized solar cells: Scale up and current–voltage characterization. *Sol. Energy Mater Sol. Cells.* **91**, 1676–1680 (2007)


## Acknowledgments

The research was supported by the Ministry of Science and Technology (MOST) of Taiwan (101-2628-E-002-015-MY3 and 103-2923-E-002-008-MY3), National Taiwan University (103R7842 and 103R7740), and Center of Strategic Materials Alliance for Research and Technology (SMART Center), National Taiwan University (102R104100).

## Author contributions

S.H. and K.W. conceived, coordinated the research, and analyzed data. C.L., H.C. and S.H. contributed to the sample fabrication and synthesis. R.S. and Y.Y. contributed to the SEM and TEM images. N.S. contributed to figures revision. The manuscript was primarily written by S.H. and revised by K.W. and K.H. All authors contributed to discussions and manuscript review.

## Additional information

**Supplementary information** accompanies this paper at http://www.nature.com/scientificreports

**Competing financial interests:** The authors declare no competing financial interests.

**How to cite this article:** Hsu, S.-H. *et al.* Platinum-Free Counter Electrode Comprised of Metal-Organic-Framework (MOF)-Derived Cobalt Sulfide Nanoparticles for Efficient Dye-Sensitized Solar Cells (DSSCs). *Sci. Rep.* **4**, 6983; DOI:10.1038/srep06983 (2014).